Unsteady Analysis of Blade and Tip Heat Transfer as Influenced by the Upstream Momentum and Thermal Wakes

Ali A. Ameri
Department of Aerospace Engineering,
Ohio State University,
Columbus, OH 43210

David L. Rigby
ASRC Aerospace,
NASA Glenn Research Center,
Cleveland, OH 44135

Erlendur Steinthorsson
A and E Consulting,
Westlake, OH 44140

James Heidmann

John C. Fabian

NASA Glenn Research Center,
Cleveland, OH 44135

The effect of the upstream wake on the time averaged rotor blade heat transfer was numerically investigated. The geometry and flow conditions of the first stage turbine blade of GE's E^3 engine with a tip clearance equal to 2% of the span were utilized. The upstream wake had both a total pressure and temperature deficit. The rotor inlet conditions were determined from a steady analysis of the cooled upstream vane. Comparisons between the time average of the unsteady rotor blade heat transfer and the steady analysis, which used the average inlet conditions of unsteady cases, are made to illuminate the differences between the steady and unsteady calculations. To help in the understanding of the differences between steady and unsteady results on one hand and to evaluate the effect of the total temperature wake on the other, separate calculations were performed to obtain the rotor heat transfer and adiabatic wall temperatures. It was found that the Nusselt number distribution for the time average of unsteady heat transfer is invariant if normalized by the difference in the adiabatic and wall temperatures. It appeared though that near the endwalls the Nusselt number distribution did depend on the thermal wake strength. Differences between steady and time averaged unsteady heat transfer results of up to 20% were seen on the blade surface. Differences were less on the blade tip surface.
[DOI: 10.1115/1.3213549]

1 Introduction

Improvement in the accuracy of the computation of heat transfer on the blade surface is essential to the design of enhanced turbine components. As turbine flows are unsteady, the question arises as to whether the average of unsteady heat load computations is significantly different from steady computations. This is nearly impossible to ascertain experimentally as the equivalent steady conditions are very difficult to configure in a turbine rig. The differences in the results of unsteady and steady computations are however possible to assess and thus help decide if the significant expenditure of additional computational resources would be justified. Such unsteady computations can be made in various modes. The most practical of them is the use of unsteady Reynolds-averaged Navier–Stokes (URANS) analysis, which has been done here. Such models are closed using a turbulence model. An additional assumption made is that these models do in fact represent the mutual effect of flow and turbulence by treating the turbulence variables as time dependent (adding a d/dt term) without any additional modeling.

Review of the earlier literature on URANS calculations of blade heat transfer as affected by the rotor/stator interaction would reveal the work of Rao et al. [1], who used a 2:3 vane to rotor blade count and a 2D code to simulate the unsteady pressure and heat transfer. In fact, the experimental work, which was carried further to different vane/blade axial spacings, as reported by Dunn et al. [2], was specifically designed with 45 rotor blades and 30 stator blades to provide a database for numerical verification. Most turbine data come from rigs, which are not as accommodating to computational fluid dynamics (CFD) methods. In the absence of such convenience, Michelassi et al. [3] rescaled the blade to maintain a one to one ratio of the vane/blade count and used a 3D methodology to calculate the blade heat transfer. Abhari et al. [4] used the 2D code UNSFLO, which uses a transformed Euler scheme to accommodate the vane to blade count ratio to compute the rotor stator interaction in a quasi-3D manner. The viscous layer was computed using a thin layer approximation and an algebraic turbulence model was used. Dunn et al. [2] studied the effect of vane/blade spacing on both the vane and blade for three different spacings. The study was performed for the midspan. They measured the unsteady heat flux and computed the same using a 2D computer program UNSFLO.

In Ref. [5] Ameri et al. used a simple analysis to determine the effect of wake unsteadiness on a "sliver" of the blade without accounting for the three-dimensional effects. This was done partly to study the effect of blade passing frequency on the blade heat transfer. They explored the results of a 1:1 vane/blade simplification and comparison to a 2:3 vane/blade count, which was a more accurate representation of the vane/blade count ratio and found the average heat transfer not to be sensitive to the vane/blade ratio in the range studied. We use the results of that study to simplify our computations. An earlier work involving the losses in unsteady wake-turbine blade interactions reported by Hodson and Dawes [6] used a two-dimensional slice and used a 1:1 ratio based on the conclusion that the effect of the passing frequency was small.

In addition to the measurements done in various works by Dunn et al., as mentioned above, there are many other experimental works that measure the unsteady blade passage heat transfer. For example, Denos et al. [7] and Chana et al. [8], each, have made heat transfer measurements in a rotating stage. In the work of Denos et al., the authors presented heat transfer measurements on the blade surface and considered the effect of rotation rate, while in the work of Chana et al., the effect of cooling of the vane on the rotor blade heat transfer was examined. The increase in the rotation rate [7] was shown to advance the location of transition upstream on the rotor blade suction surface and increase the level of

Contributed by the International Gas Turbine Institute of ASME for publication in the JOURNAL OF TURBOMACHINERY. Manuscript received August 28, 2008; final manuscript received February 9, 2009; published online April 29, 2010. Review conducted by David Wisler. Paper presented at the ASME Turbo Expo 2008: Land, Sea and Air (GT2008), Berlin, Germany, June 9–13, 2008.

heat transfer on the pressure side. This increase in the pressure side heat transfer could be due to the increased buffeting by the wake or due to a change in the relative inlet angle although the latter possibility has been discounted in Ref. [7].

In an earlier work, Ameri et al. [9] computed the surface and tip heat transfer coefficients for rotating blades of the first stage high-pressure turbine of GE E^3. The present is the culmination of the work presented in Refs. [5,9]. The computations in Ref. [9] are used in this paper but constitute a subset of the computations utilized, as will be discussed later in this work.

2 Computational Preliminaries

The computer code used for this study was GLENN-HT2000. The numerical procedure uses a finite-volume discretization scheme that is second order accurate in time and space. An implicit time marching scheme is implemented using subiterations. The turbulence model used for the calculations was the low Reynolds number k-ω model of Wilcox [10], which integrates to the walls (i.e., without the use of wall-functions). The grid used was quite fine. Maximum grid spacing in the layer adjacent to the wall was such that maximum value of y^+ was less than unity. The turbulence model is able to produce an effect similar to the transition from laminar to turbulent flow. In practice, however, the transition is not guaranteed to be in the appropriate location. In fact, it is often triggered very near the leading edge, which is what occurred in our computations, making them turbulent except near the stagnation line. Further details about the code may be found in Ref. [11]. The present version of the computer code is fully parallelized and uses Message Passing Interface (MPI) for parallel processing. The three-dimensional cases were run on 48 processors of a 98 processor Xeon Linux Cluster.

2.1 The Geometry and Conditions. Over the years, the NASA/GE E^3 geometry and conditions have become popular cases to simulate. The reasons for this are that the geometry is for a modern design configuration and that it is freely available. We have made use of this geometry [12] in our earlier work and have used it for the present work. The geometry and flow conditions of the first stage turbine blade have been used to obtain the three-dimensional blade and tip heat transfer [11,13] for various tip/casing treatments. There is a good deal of confidence associated with results in Refs. [11,13] for two reasons. First, the numerical scheme has been experimentally validated for tip heat transfer computations in Refs. [14,15]. Second, the blade has been adopted and used by other researchers. As such, much of the results found in Refs. [11,13] have also been independently verified using other codes. Two of such computations may be found in Refs. [16,17].

For this work, the effect of the upstream wake of the first-stage vane on the blade heat transfer was simulated. The blade tip clearance was 2% of the blade span. There were 46 vanes and 76 blades or a vane/blade ratio of approximately 0.61. The blade was rotating at 8400 rpm. The pressure ratio across the rotor blade was set to the stage pressure ratio of 0.44 (assuming no loss in the stator passage.) The vane flow was computed separately as will be described subsequently.

2.2 Vane Computation and the Wake Shape. The guide vane flow was computed using the same code in steady mode. The pressure ratio was 0.59 at the exit of the computational domain at the hub. A specific heat ratio of 1.36 was used for the stage. The wall temperature was specified as 0.7 times the inlet total temperature to make the conditions representative of the real flow conditions. The total pressure and temperature thus computed are shown in Fig. 1. The wakes were taken from the midspan and were generalized to the whole plane of the inlet of the blade. The total pressure in the wake thus produced was approximated with a trigonometric function as follows:

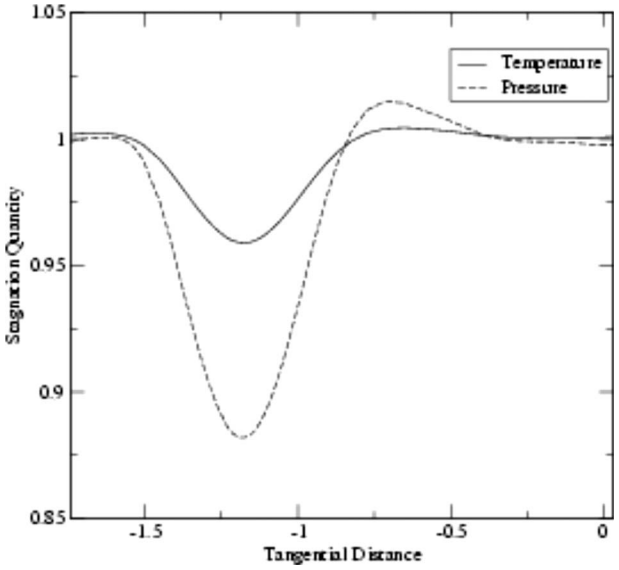

Fig. 1 Total pressure and temperature at the exit

$$P_0(t,\theta) = P_{0-bg}\left\{1. - 0.15\left[\sin\left(\frac{n\theta}{2} + \frac{\pi t}{\tau}\right)\right]^{10}\right\} \tag{1}$$

where the subscript bg designates the background value, which is a function of radial position only. As for the thermal wake behind the vane the expression used was

$$T_0(t,\theta) = T_{0-bg}\left\{1. - 0.05\left[\sin\left(\frac{n\theta}{2} + \frac{\pi t}{\tau}\right)\right]^{10}\right\} \tag{2}$$

The total pressure and temperature profiles were merged with endwall turbulent boundary layer profiles on the hub and case, which were 1% of the span at the inlet.

The wake turbulence and length scale were also approximately fitted with trigonometric functions and specified at the inlet. The background level for turbulence intensity was 2% and the amplitude was 3% for a peak value of 5%, i.e.,

$$Tu(t,\theta) = Tu_{bg} + Tu_{\text{amp}}\left[\sin\left(\frac{n\theta}{2} + \frac{\pi t}{\tau}\right)\right]^6 \tag{3}$$

The same applies to the length scale with a background level of $0.01C_x$ and a peak of $0.025C_x$. The average inlet turbulence was computed to be 2.6% with an average length scale of $0.015C_x$. It should be noted that the turbulence intensity as specified at the inlet was normalized by the absolute freestream velocity. As a fraction of the relative velocity, the average inlet turbulence level was about 7%. This was because, at the midspan, the inlet absolute velocity approached the blade at 75 deg and the relative velocity's approach was at approximately 45 deg thus yielding 2.7 as the ratio of the absolute velocity to the relative velocity.

2.3 Further Simplifications. To reduce the cost of the computations, a wake-passing frequency corresponding to a one to one vane/blade ratio was used. This simplification was based upon a separate preliminary study reported in Ref. [5], which showed that for the purposes of computing the average heat transfer, the wake frequency for a 1:1 ratio produces a very similar result as compared with a 2:3 ratio. The 2:3 ratio is an approximation to the actual vane/blade count, which was 46:76. It should be noted that this approximation does not change the number of rotor blades. It only increases the frequency of wake-passing.

2.4 The Grid. Figure 2 shows the blade and hub endwall surface as represented by the grid used for the three-dimensional computations performed in this work. The grid contained 164 blocks and had a total of 1.8 million nodes. There were 65 nodes

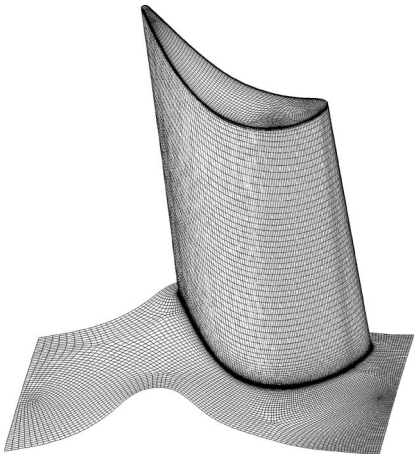

Fig. 2 Grid on blade hub and surfaces

across the tip gap in the radial direction. The large number of grid points across the tip of the blade was necessitated by the grid topology, which was designed not to needlessly spread the grid points in the freestream where this often causes slowness of convergence. The grid density from the hub to the tip was 101 nodes. The grid topology though unstructured, it contains blocks that are structured. The grid density was arrived at after running exploratory computations. The grid was deemed sufficiently refined when able to support a wake without it dissipating. A dimensionless time step of 0.005 was used after comparing results using time steps of 0.001, 0.0025, 0.005, and 0.01. The results showed that the time histories for the first three time steps were identical, while the larger 0.01 deviated from that time history. The larger time step of 0.005 also resulted in fewer total subiterations and faster convergence. For the chosen time step size, there were 320 time steps required to cover the passing of a wake across a single blade passage, which is much finer than the resolution commonly used for this purpose. To obtain a converged unsteady solution, the local blade heat transfer was monitored and convergence was declared only when local blade heat transfer became periodic and the magnitude of the variations attained a constant level.

3 Results and Discussion

3.1 Blade Surface Heat Transfer

3.1.1 Unsteady Heat Transfer. In Fig. 3, we present the unsteady variation in heat transfer rate in the form of normalized heat flux on the blade surface. We have shown four different snapshots within a period of a wake-passing going from left to the right and repeating again. On the suction side (top row), a large patch of high heat transfer continuously moves downstream on the surface. Time periodic behavior is also apparent near the hub and on the tip of the blade. On the pressure side (bottom row), the periodic behavior is again apparent. A low heat transfer patch starts upstream, moves downstream, and spreads. Still farther in time, it retracts and reduces to the small area upstream. There is obviously an unsteady variation in blade heat transfer. The question is whether this variation is, on the average, significant.

Recently, in Ref. [9], we computed the unsteady rate of heat transfer for the present configuration as influenced by the vane's momentum wake. We did not include the effect of the thermal wake. We found that the unsteady effect on the blade, as measured by the percent difference between the average of the unsteady and equivalent steady conditions on the blade surface, was somewhat significant. This difference was quite small on the blade tip. In the present computations, we have included the thermal wake. We have, in this work, computed the heat transfer coefficient using the adiabatic wall temperature to gauge the effect of the thermal wake on the heat transfer coefficient. This has been done for the case of nonthermal wake (momentum wake only) and with the thermal wake. In order to compute for the heat transfer coefficient, two separate calculations were performed. In the first one a constant temperature boundary condition of $T_w=0.7$ was used. From this, the wall heat flux was computed. In order to compute the heat transfer coefficient, which would be independent of the wall tem-

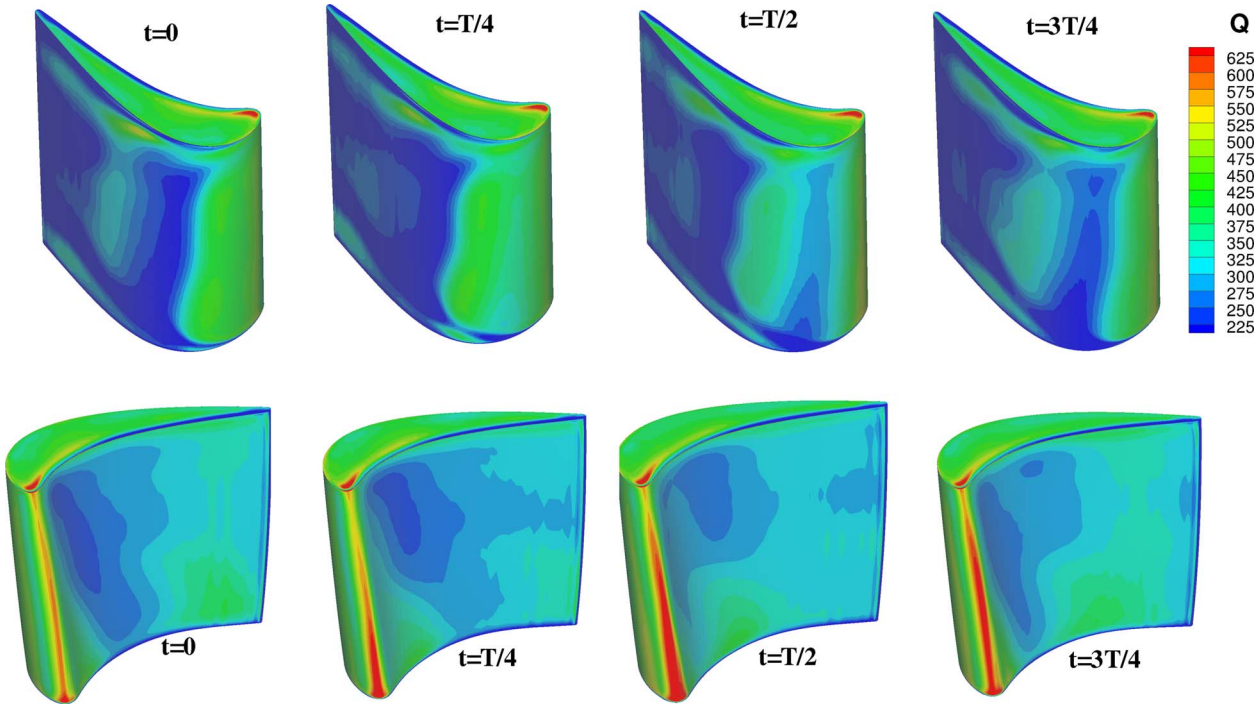

Fig. 3 Blade surface heat flux at four equally spaced times in a period of wake-passing; top row shows the suction side, and the bottom row shows the pressure side

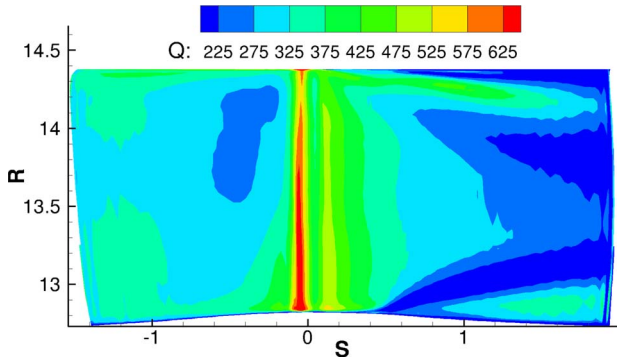

Fig. 4 Distribution of the average wall heat flux on the blade surface (w/o thermal wake)

perature, and, as well, insensitive to the local "bulk" temperature, the adiabatic wall temperature was computed. This was accomplished by setting the wall heat flux to zero and computing the unsteady wall temperature. Unsteady heat flux along with the unsteady adiabatic wall temperature and the unsteady heat transfer coefficient were averaged and are presented below.

In Figs. 4–12, which present the blade surface results, we have shown both the suction and pressure sides of the blade and variables are plotted along the distance over the blade surface measured from the minimum axial distance. The positive side is the suction side and the negative side is the pressure side. The ordinate is the radial direction.

To start, in Figs. 4–6 the no thermal wake case in Ref. [9] is revisited and the time averages of the adiabatic temperature and Nusselt number distribution are evaluated and presented. The importance of this exercise will be expounded after the results are shown.

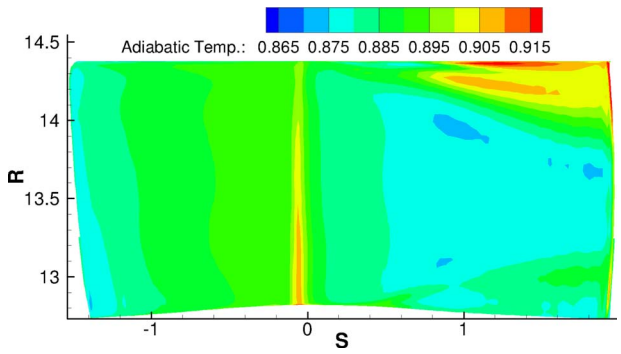

Fig. 5 Distribution of the average adiabatic wall temperature over the blade surface (w/o thermal wake)

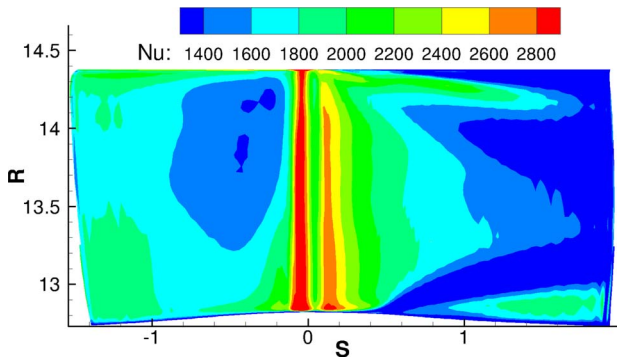

Fig. 6 Average heat transfer coefficient distribution over the blade surface (w/o thermal wake)

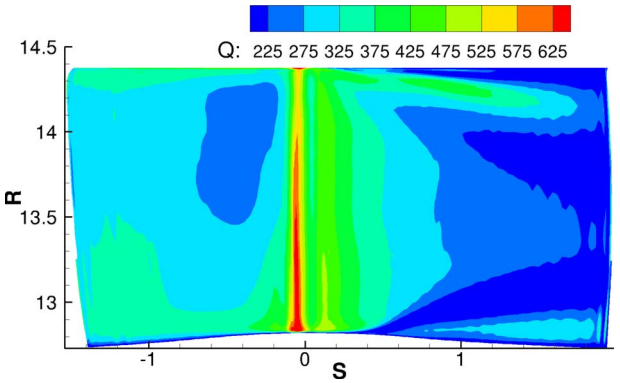

Fig. 7 Distribution of the average wall heat flux on the blade surface (with thermal wake)

Figure 4 presents the average heat flux. As expected, the heat flux is largest around the leading edge near the tip, where the tip clearance vortex is active, and on the pressure side near the tip, where the "sink" effect is most pronounced. Figure 5 shows the time average of the adiabatic wall temperature. It is interesting to observe that on the suction side near the tip, the adiabatic wall temperature (Fig. 5) is as high as than the values observed near the hub and around the leading edge. At this location near the tip, T_{aw} is the highest on the blade. This is because the fluid flowing along that part of the blade passage has gone over the tip and has not done any work, thus maintaining a total temperature that is near the absolute stage total temperature. This would lead to elevated wall temperatures that would need to be accounted for in the thermal management of the blade. Computed also is the heat

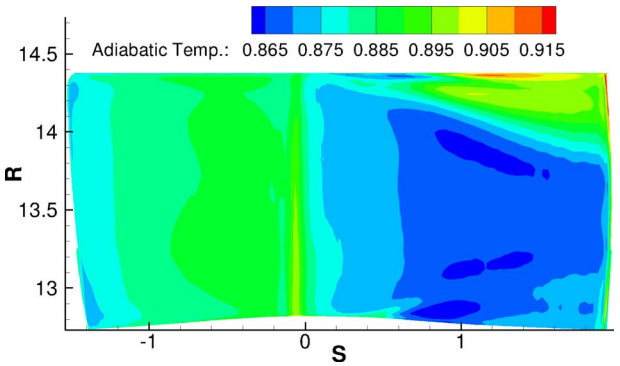

Fig. 8 Distribution of the average adiabatic wall temperature over the blade surface (with thermal wake)

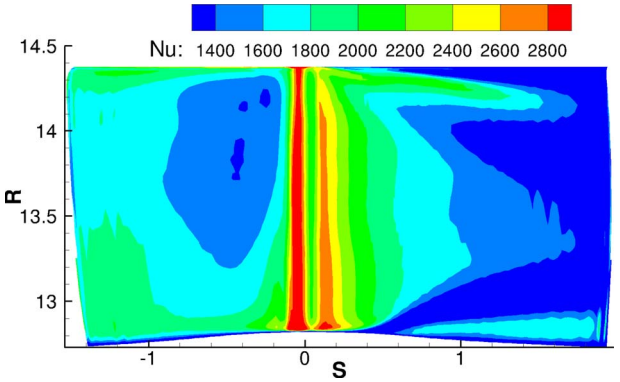

Fig. 9 Average heat transfer coefficient distribution over the blade surface (with thermal wake)

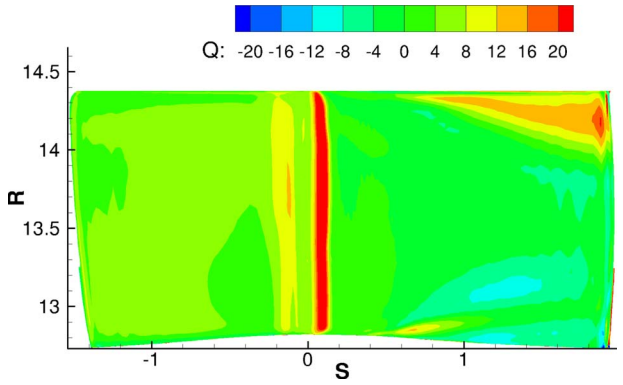

Fig. 10 Percent difference between the unsteady average and steady computation of the heat flux

transfer coefficient. The unsteady wall heat flux and unsteady local adiabatic wall temperature, which are in phase with respect to the inlet wake variation, are used to compute for the heat transfer coefficient.

$$h = Q_w/(T_w\text{-}T_{aw}) \tag{4}$$

The heat transfer coefficient, which is nondimensionalized in the form of the Nusselt number, is shown in Fig. 6. It was computed by averaging the Nu over a wake-passing period. Plots of the results of the computations, which include both the momentum and thermal wakes, are presented in Figs. 7–9. The heat flux and adiabatic wall temperature are commensurately lower than the case without the thermal wake. Experimentally, it has been shown by Chana et al. [8] that the presence of the thermal wake resulting from cooling the vane surface leads to a reduction in the blade

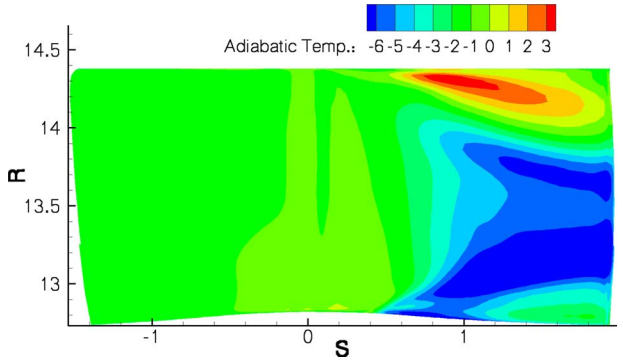

Fig. 11 Percent difference between the unsteady average and steady adiabatic wall temperature

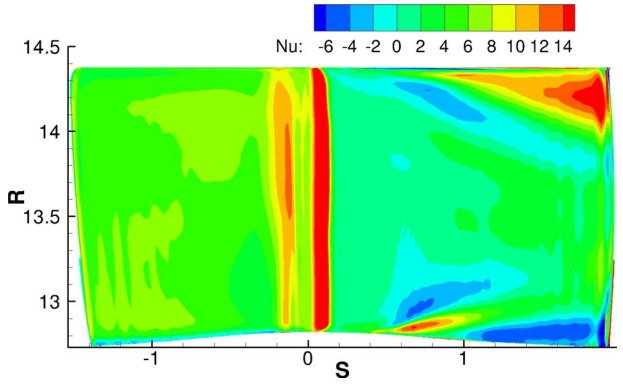

Fig. 12 Percent difference between the unsteady average and steady heat transfer coefficient

surface heat transfer. This, as they explain, is caused by a reduction in the bulk temperature. They do not present the effect of the thermal wake in terms of the Nusselt number but the unscaled thermal flux in Figs. 4 and 7 agree with that conclusion. The heat transfer coefficient distribution, as shown by the Nusselt number in Figs. 6 and 9, are nearly identical if it were not for the near hub on the suction side. A dissimilarity of the Nusselt number distribution would suggest a difference in the flow physics, which could be brought about by, say, thermal segregation akin to what has been suggested as taking place when hot streaks are present [18]. Such segregation is caused, as suggested by Kerrebrock and Mikolajczak [19], by a deviation in the inlet angle from the dominant inlet angle due to variation in the freestream temperature of a constant Mach number stream, and thus, resulting in changes in the relative velocity. A detailed analysis was also performed by Shang and Epstein [20].

3.1.2 Steady Flow Conditions. The results derived from the unsteady computations are now compared with those from a set of steady computations. Again, two computations were made: one using an adiabatic boundary condition to compute the adiabatic wall temperature distribution and another to compute for the wall heat flux at a fixed wall temperature. To make the conditions equivalent, the inlet total pressure and temperature averages over a wake-passing period were computed from the wake profiles and assigned as inlet conditions to the steady computations. Results of the computations were plotted in a similar manner, as shown in Figs. 4–9 (not shown here), which yielded like patterns and again invariance in the Nusselt number distribution. Instead of presenting the results of the steady computations, the differences between the steady and unsteady computations, and only for the case in which both the wakes are present, will be shown.

3.1.3 Difference Between Unsteady and Steady Computations. Figure 10 shows the percent difference in the heat flux between the average of the unsteady wall heat flux and steady heat flux. It is defined as $\bar{Q}-Q/\bar{Q}\times 100$. The differences are similar to that reported in Ref. [9], where the unsteady average of the heat flux is up to 20% higher than the steady average. This agrees with the results of Denos et al. [7], which show increase in the pressure side heat transfer with increase in the rotation rate. This may be attributable to an increase in the buffeting rate, which is responsible for the increase in the pressure side heat transfer if not due to a net change in the inlet relative angle.

The difference in the adiabatic wall temperature is defined as $\overline{Taw}-Taw/\overline{Taw}-\overline{Tw}\times 100$. Here, the overbar denotes time averaged quantity and the numerator is the difference between the unsteady average and the steady value. As shown in Fig. 11, the difference appears to be small as a percentage of the difference in the average adiabatic wall and wall temperatures. The distribution explains some of the change in the heat flux, which is due to the change in the adiabatic wall temperature. The difference in the Nusselt number based on the heat transfer coefficient defined in Eq. (4) is presented in Fig. 12. It is defined using the unsteady average and steady values of the Nusselt number as $\frac{\overline{Nu}-Nu}{\overline{Nu}}\times 100$. The large difference near the leading edge is attributable to the differences in the start of transition, which occurs somewhat earlier with the wake induced unsteadiness. This difference in the leading edge heat transfer and to a lesser extent on the pressure side of the blade was eliminated in Ref. [9] by adjusting the turbulence intensity upwards, namely, from an average of 2.6–3%. The differences in the heat transfer in other areas were not affected by the adjustment in turbulence intensity. The largest difference is shown to be near the tip on the suction side. As shown in Fig. 12, the difference in the Nusselt number is as much as 20% on the suction side near the tip. On the pressure side, this difference is up to 8%, and is consistently higher than the steady results. On the suction side, there are areas of negative difference but they are matched with positive areas, thus representing a shift and not

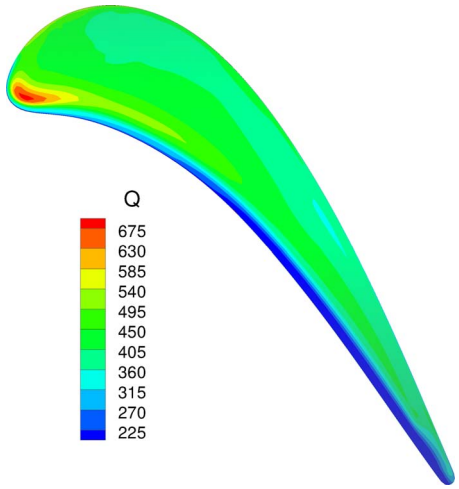

Fig. 13 Average of the unsteady heat flux

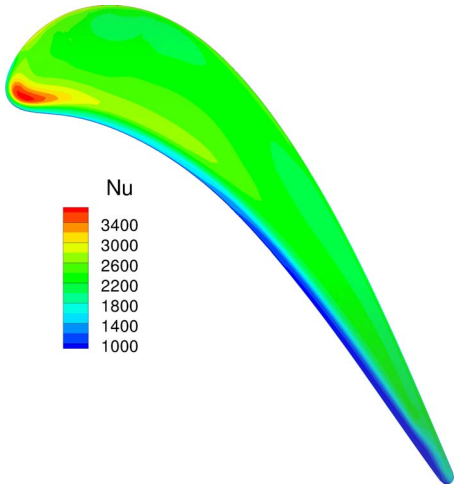

Fig. 15 Average of the unsteady Nusselt number

a net change. The pictures show that the difference in the heat flux is partly due to the change in the thermal potential and partly due to a change in the flow, which is represented by the Nusselt number distribution. For example, the increase in the heat flux near the tip on the suction side toward the trailing edge is entirely due to an increase in the Nusselt number, while upstream, nearer to the tip, the increase is due to a combination of the increases in the Nusselt number and thermal potential.

3.2 Tip Heat Transfer

3.2.1 Unsteady Average. The time average of unsteady tip heat transfer measured by the normalized heat flux, adiabatic wall temperature, and the heat transfer coefficient of Eq. (4) are presented in Figs. 13–15. Only the condition with both wakes is presented. The adiabatic wall temperature distribution is remarkably flat and suggests a lower recovery temperature as compared with the blade surface. The patterns of heat flux distribution are as described for example in Refs. [13,14]. The heat transfer coefficients are elevated as compared with the blade surface.

3.2.2 Difference of Unsteady Average and Steady Distributions. Figures 16 and 17 show the percent difference between the average of the unsteady and steady computations as defined earlier for the blade surface. The differences are seen to be quite small both for the adiabatic wall temperature and for the Nusselt number. These differences lead to differences in the heat

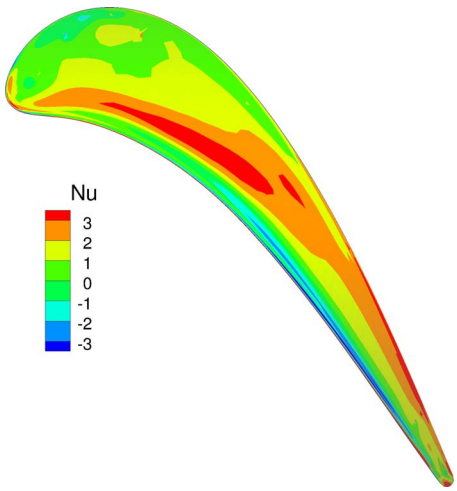

Fig. 16 Percent deviation from the average of the unsteady Nusselt number

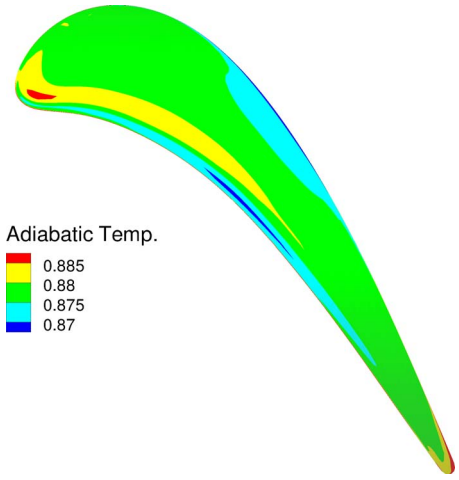

Fig. 14 Average of the unsteady adiabatic wall temperature

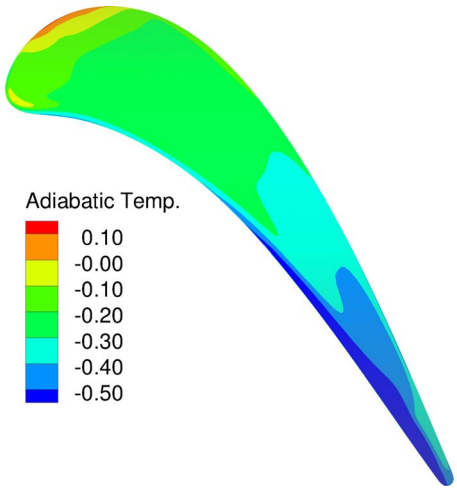

Fig. 17 Percent deviation from the average of the unsteady adiabatic wall temperature

flux of at most around 4% and mostly positive over the tip surface. The conclusions agree with the findings in Ref. [9], which did not show a large difference in the results obtained from unsteady and steady analyses both for heat flux and pressure on the blade tip at this intermediate tip clearance.

4 Summary and Conclusions

It seems likely that the URANS result could generally be more accurate than RANS. More of the scales are resolved using URANS and the unsteadiness resolved with URANS is coherent and periodic; this is not the type of unsteadiness that characterizes turbulence and more likely to be resolved by unsteady analysis. We set out to address the question of whether a URANS analysis would result in a significantly different convective heat transfer coefficient compared with a steady analysis. The wake was simulated using a gust type boundary condition. Rotor blade surface heat flux and adiabatic wall temperature, as influenced by the momentum and thermal wakes behind the vane, were computed. This required two separate computations, either steady or unsteady, to be made and the results processed in a phase locked fashion.

The Nusselt number, which is the blade heat transfer flux scaled with $(T_{aw}-T_w)$, appears to be mostly the same for both the steady computations and for the average of the unsteady computations. Some differences are observable, which we have attributed to the phenomenon of thermal segregation.

The adiabatic wall temperature on the suction side near the tip and toward the trailing edge was found to be the highest on the blade surface. This rise in the adiabatic wall temperature would give rise to higher surface temperatures in this area, which is what is seen in engines. The unsteady computations of heat transfer coefficient generally yielded higher values than the steady values for the blade pressure side by as much as 8%. On the suction side, the difference was as high as 20% near the tip close to the trailing edge. The net difference was positive on the suction side. There were negative differences but those were caused by a shift.

Concerning the tip heat transfer, the maximum difference between the unsteady and steady computations was about 4% in the middle of blade tip.

Some differences were observed in the Nusselt number distribution for unsteady flow computations, depending on whether or not the thermal wake was included. This difference was limited to the suction side and close to the hub.

4.1 Recommendation for Stage Heat Transfer Computations. The dissimilarity in the adiabatic wall temperature suggests that, for stage unsteady computations, the adiabatic wall temperature for the rotor be computed with the stator set to nonadiabatic boundary condition (cooled) because of the effect of the thermal wake on the rotor blade adiabatic wall temperature. In other words, a computation of the adiabatic wall temperature with both the stator and rotor set to adiabatic conditions would yield adiabatic wall temperature on the rotor that would not be appropriate. For multiple stages, when computing for a blade's adiabatic wall temperature, all the upstream blades and vanes must be set to cooled (nonadiabatic.) To compute for the Nusselt number, the adiabatic wall temperature and wall heat flux must be computed under similar freestream conditions, which includes thermal conditions.

Nomenclature

C = axial chord
h = heat transfer coefficient$=q_w/(T_{aw}-T_w)$
K = reference thermal conductivity
Nu = Nusselt Number$=hC/k$
n = number of vanes per row
P = pressure
q = wall heat flux
Q = heat flux nondimensionalized by K_0T_0/C
R = local radius
S = wetted distance along the blade, positive on the suction side and negative on the pressure side
t = time
Tu = turbulence intensity
T = temperature normalized by the inlet freestream absolute temperature

Greek

θ = local tangential angle
τ = time period for one wake passage

Subscripts

0 = absolute total value
a = adiabatic
amp = amplitude
bg = background value
w = wall value
x = axial value

References

[1] Rao, K. V., Delaney, R. A., and Dunn, M. G., 1994, "Vane-Blade Interaction in a Transonic Turbine, II—Heat Transfer," J. Propul. Power, **10**(3), pp. 312–317.
[2] Dunn, M. G., Haldeman, C. W., Abhari, R. S., and McMillan, M. L., "Influence of Vane/Blade Spacing on the Heat Flux for a Transonic Turbine," ASME Paper No. 2000-GT-0206.
[3] Michelassi, V., Martelli, F., Deons, R., Arts, T., and Sieverding, C. H., 1999, "Unsteady Heat Transfer in Stator-Rotor Interaction by Two-Equation Turbulence Mode," ASME J. Turbomach., **121**, pp. 436–447.
[4] Abhari, R. S., Guenette, G. R., Epstein, A. H., and Giles, M. B., 1992, "Comparison of Time-Resolved Turbine Rotor Blade Heat Transfer Measurements and Numerical Calculations," ASME J. Turbomach., **114**(4), pp. 818–827.
[5] Ameri, A. A., Rigby, D., Heidmann, J., Steinthorsson, E., and Fabian, J., 2006, "Effects of Unsteadiness Due to Wake Passing on Rotor Blade Heat Transfer," AIAA Paper No. AIAA-2006-3263.
[6] Hodson, H. P., and Dawes, W. N., 1998, "On the Interpretation of Measured Profile Losses in Unsteady Wake-Turbine Blade Interaction Studies," ASME J. Turbomach., **120**, pp. 276–284.
[7] Denos, R., Sieverding, C. H., Arts, T., Brouckaert, J., Paniagua, G., and Michelassi, V., 1999, "Experimental Investigation of the Unsteady Rotor Aerodynamics of a Transonic Turbine Stage," Third European Conference in Turbomachinery, Fluid Dynamics and Thermodynamics (IACA Programme).
[8] Chana, K. S., Hilditch, M. A., and Anderson, J. A., 2005, "An Investigation of the Effects of Film Cooling in a High-Pressure Aeroengine Turbine Stage," ASME Paper No. GT-2005-68564.
[9] Ameri, A. A., Rigby, D. L., Steinthorsson, E., Heidmann, J., and Fabian, J. C., 2007, "Numerical Simulation of Unsteady Turbine Blade and Tip Heat Transfer Due to Wake Passing," ASME Paper No. GT2007-27550.
[10] Wilcox, D. C., 1994, *Turbulence Modeling for CFD*, DCW Industries, Inc., La Canada, CA.
[11] Ameri, A. A., Steinthorsson, E., and Rigby, D., 1998, "Effect of Squealer Tips on Rotor Heat Transfer and Efficiency," ASME J. Turbomach., **120**(4), pp. 753–759.
[12] Halila, E. E. and Lenahan, D. T., and Thomas, L. L., 1982, "Energy Efficient Engine, High Pressure Turbine Test Hardware Detailed Design Report," NASA Report No. CR-167955.
[13] Ameri, A. A., Steinthorsson, E., and Rigby, D., 1999, "Effect of Tip Clearance and Casing Recess on Heat Transfer and Stage Efficiency in Axial Turbines," ASME J. Turbomach., **121**(4), pp. 683–693.
[14] Ameri, A. A., and Bunker, R. S., 2000, "Heat Transfer and Flow in the First Stage Blade Tip of a Power Generation Gas Turbine, Part 2: Analytical Results," ASME J. Turbomach., **122**, pp. 272–277.
[15] Ameri A. A., 2001, " Heat Transfer and Flow on the Blade Tip of a Gas Turbine Equipped With a Mean-Camberline Strip," ASME J. Turbomach., **123**(4), pp. 704–708.
[16] Mumic, F., Eriksson, D., and Sunden, B., 2004, "On Prediction of Tip Leakage Flow and Heat Transfer in Gas Turbines," ASME Paper No. GT2004-53448.
[17] Yang, D.-L., and Feng, Z.-P., 2007, "Tip Leakage Flow and Heat Transfer Predictions for Turbine Blade," ASME Paper No. GT2007-27728.
[18] Dorney, D. J., Davis, R. L., Edwards R. L., and Madavan N. K., 1992, "Unsteady Analysis of Hot Streak Migration in a Turbine Stage," J. Propul. Power, **8**(2), pp. 520–529.
[19] Kerrebrock, J. L., and Mikolajczak, A. A., 1970, "Intra-Stator Transport of Rotor Wakes and Its Effect on Compressor Performance," ASME J. Eng. Power, **92**(4), pp. 359–368.
[20] Shang, T., and Epstein, A. H., 1997, "Analysis of Hot Streak Effects on Turbine Rotor Heat Load," ASME J. Turbomach., **119**, pp. 544–553.